RESEARCH ARTICLE SUMMARY

ASTEROIDS

The geomorphology, color, and thermal properties of Ryugu: Implications for parent-body processes

S. Sugita*, R. Honda, T. Morota, S. Kameda, H. Sawada, E. Tatsumi, M. Yamada, C. Honda, Y. Yokota, T. Kouyama, N. Sakatani, K. Ogawa, H. Suzuki, T. Okada, N. Namiki, S. Tanaka, Y. Iijima, K. Yoshioka, M. Hayakawa, Y. Cho, M. Matsuoka, N. Hirata, N. Hirata, H. Miyamoto, D. Domingue, M. Hirabayashi, T. Nakamura, T. Hiroi, T. Michikami, P. Michel, R.-L. Ballouz, O. S. Barnouin, C. M. Ernst, S. E. Schröder, H. Kikuchi, R. Hemmi, G. Komatsu, T. Fukuhara, M. Taguchi, T. Arai, H. Senshu, H. Demura, Y. Ogawa, Y. Shimaki, T. Sekiguchi, T. G. Müller, A. Hagermann, T. Mizuno, H. Noda, K. Matsumoto, R. Yamada, Y. Ishihara, H. Ikeda, H. Araki, K. Yamamoto, S. Abe, F. Yoshida, A. Higuchi, S. Sasaki, S. Oshigami, S. Tsuruta, K. Asari, S. Tazawa, M. Shizugami, J. Kimura, T. Otsubo, H. Yabuta, S. Hasegawa, M. Ishiguro, S. Tachibana, E. Palmer, R. Gaskell, L. Le Corre, R. Jaumann, K. Otto, N. Schmitz, P. A. Abell, M. A. Barucci, M. E. Zolensky, F. Vilas, F. Thuillet, C. Sugimoto, N. Takaki, Y. Suzuki, H. Kamiyoshihara, M. Okada, K. Nagata, M. Fujimoto, M. Yoshikawa, Y. Yamamoto, K. Shirai, R. Noguchi, N. Ogawa, F. Terui, S. Kikuchi, T. Yamaguchi, Y. Oki, Y. Takao, H. Takeuchi, G. Ono, Y. Mimasu, K. Yoshikawa, T. Takahashi, Y. Takei, A. Fujii, C. Hirose, S. Nakazawa, S. Hosoda, O. Mori, T. Shimada, S. Soldini, T. Iwata, M. Abe, H. Yano, R. Tsukizaki, M. Ozaki, K. Nishiyama, T. Saiki, S. Watanabe, Y. Tsuda

INTRODUCTION: The asteroid 162173 Ryugu is the target of the Japanese Hayabusa2 mission, which is designed to collect samples from Ryugu's surface and return them to Earth. We seek to understand Ryugu's formation from a parent body, both to better explain the origin of near-Earth asteroids and to provide context for analyzing the samples. Theoretical calculations indicate that Ryugu-size asteroids are likely produced through catastrophic disruption of a parent body, formed in the early Solar System, whose fragments then reaccumulated. Ryugu later migrated from the main asteroid belt to its current near-Earth orbit.

RATIONALE: Hayabusa2 rendezvoused with the asteroid in June 2018. Detailed global observations of Ryugu were conducted with Hayabusa2's remote-sensing instruments, including the optical navigation cameras (ONCs), laser altimeter [light detection and ranging (LIDAR) altimeter], and a thermal infrared camera (TIR). We examined the asteroid's surface colors, geomorphological features, and thermal properties to constrain models of its formation.

RESULTS: Geologic features on Ryugu include a circum-equatorial ridge, an underlying east-west dichotomy, high boulder abundance, impact craters, and large-scale color uniformity.

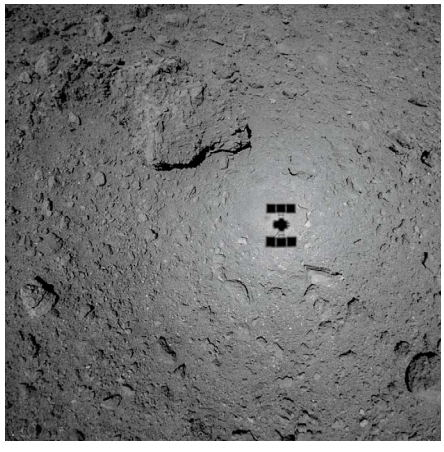

Hayabusa2's shadow on the surface of asteroid Ryugu. The shadow of the solar panels spans 6 m. The bright halo is due to the opposition effect, which enhances the reflectance at small solar phase angles.

We estimate that the impact craters penetrating the top 10 meters of Ryugu's surface have existed for 10^7 to 10^8 years, indicating that the last major resurfacing likely occurred while Ryugu was still located in the main asteroid belt. In contrast, the low number density of small craters (~10 m in diameter) suggests a very young resurfacing age ($\lesssim 10^6$ years) for the top 1-meter layer.

Multicolor optical observations revealed that Ryugu possesses the average spectrum of a Cb-type asteroid and lacks a ubiquitous 0.7-μm absorption band. These spectral observations and a principal components analysis suggest that Ryugu originates from the Eulalia or Polana asteroid family in the inner main belt, possibly via more than one generation of parent bodies.

Ryugu's geometric albedo at 0.55 μm is 4.5 ± 0.2%, among the lowest in the Solar System. Moderately dehydrated carbonaceous chondrites and interplanetary dust particles (IDPs) are the only meteoritic samples with similarly low albedos. The high boulder abundance and the spectral properties of the boulders are consistent with dehydrated surface materials, which might be analogous to thermally metamorphosed meteorites.

ON OUR WEBSITE

Read the full article at http://dx.doi.org/10.1126/science.aaw0422

The spectra of Ryugu's surfaces occupy a small area in the dehydration track of our principal component space, suggesting that a large volume of Ryugu's original parent body experienced similar degrees of partial dehydration. Such uniformity is more consistent with internal heating on the parent body than heating due to multiple impacts. Nevertheless, it is possible that global partial dehydration could result from impacts if the parent body sustained many impacts before its catastrophic disruption. Geochemical analyses of thermally metamorphosed meteorites are consistent with short-term heating; thus, this scenario cannot be readily discarded.

A third possibility is that Ryugu is covered with materials that experienced only incipient aqueous alteration, possibly similar to some IDPs. If so, the spectral trend observed in Ryugu's boulders may be a progression of aqueous alteration.

CONCLUSION: Multiple scenarios remain viable, but the Hayabusa2 remote-sensing data are most consistent with parent-body partial dehydration due to internal heating. This scenario suggests that asteroids formed from materials that condensed at ≤150 K (the H_2O condensation temperature under typical solar nebula conditions) must have either formed sufficiently early to contain high concentrations of radiogenic species, such as ^{26}Al, or formed near the Sun, where they experienced other heating mechanisms. The degree of internal heating would constrain the location and/or timing of the snow line (the dividing line between H_2O condensation and evaporation) in the early Solar System. ■

The list of author affiliations is available in the full article online.
*Corresponding author: Email: sugita@eps.s.u-tokyo.ac.jp
Cite this article as S. Sugita *et al.*, *Science* **364**, eaaw0422 (2019). DOI: 10.1126/science.aaw0422

RESEARCH ARTICLE

ASTEROIDS

The geomorphology, color, and thermal properties of Ryugu: Implications for parent-body processes

S. Sugita[1,2]*, R. Honda[3], T. Morota[4], S. Kameda[5], H. Sawada[6], E. Tatsumi[1], M. Yamada[2], C. Honda[7], Y. Yokota[6,3], T. Kouyama[8], N. Sakatani[6], K. Ogawa[9], H. Suzuki[10], T. Okada[6,1], N. Namiki[11,12], S. Tanaka[6,12], Y. Iijima[6]†, K. Yoshioka[1], M. Hayakawa[6], Y. Cho[1], M. Matsuoka[6], N. Hirata[7], N. Hirata[9], H. Miyamoto[1], D. Domingue[13], M. Hirabayashi[14], T. Nakamura[15], T. Hiroi[16], T. Michikami[17], P. Michel[18], R.-L. Ballouz[6,19], O. S. Barnouin[20], C. M. Ernst[20], S. E. Schröder[21], H. Kikuchi[1], R. Hemmi[1], G. Komatsu[22,2], T. Fukuhara[5], M. Taguchi[5], T. Arai[23], H. Senshu[2], H. Demura[7], Y. Ogawa[7], Y. Shimaki[6], T. Sekiguchi[24], T. G. Müller[25], A. Hagermann[26], T. Mizuno[6], H. Noda[11], K. Matsumoto[11,12], R. Yamada[7], Y. Ishihara[6]‡, H. Ikeda[27], H. Araki[11], K. Yamamoto[11], S. Abe[28], F. Yoshida[2], A. Higuchi[11], S. Sasaki[29], S. Oshigami[11], S. Tsuruta[11], K. Asari[11], S. Tazawa[11], M. Shizugami[11], J. Kimura[29], T. Otsubo[30], H. Yabuta[31], S. Hasegawa[6], M. Ishiguro[32], S. Tachibana[1], E. Palmer[13], R. Gaskell[13], L. Le Corre[13], R. Jaumann[21], K. Otto[21], N. Schmitz[21], P. A. Abell[33], M. A. Barucci[34], M. E. Zolensky[33], F. Vilas[13], F. Thuillet[18], C. Sugimoto[1], N. Takaki[1], Y. Suzuki[1], H. Kamiyoshihara[1], M. Okada[1], K. Nagata[8], M. Fujimoto[6], M. Yoshikawa[6,12], Y. Yamamoto[6,12], K. Shirai[6], R. Noguchi[6], N. Ogawa[6], F. Terui[6], S. Kikuchi[6], T. Yamaguchi[6]§, Y. Oki[1], Y. Takao[1], H. Takeuchi[6], G. Ono[27], Y. Mimasu[6], K. Yoshikawa[27], T. Takahashi[6], Y. Takei[6,27], A. Fujii[6], C. Hirose[27], S. Nakazawa[6], S. Hosoda[6], O. Mori[6], T. Shimada[6], S. Soldini[6], T. Iwata[6,12], M. Abe[6,12], H. Yano[6,12], R. Tsukizaki[6], M. Ozaki[6,12], K. Nishiyama[6], T. Saiki[6], S. Watanabe[4,6], Y. Tsuda[6,12]

The near-Earth carbonaceous asteroid 162173 Ryugu is thought to have been produced from a parent body that contained water ice and organic molecules. The Hayabusa2 spacecraft has obtained global multicolor images of Ryugu. Geomorphological features present include a circum-equatorial ridge, east-west dichotomy, high boulder abundances across the entire surface, and impact craters. Age estimates from the craters indicate a resurfacing age of $\lesssim 10^6$ years for the top 1-meter layer. Ryugu is among the darkest known bodies in the Solar System. The high abundance and spectral properties of boulders are consistent with moderately dehydrated materials, analogous to thermally metamorphosed meteorites found on Earth. The general uniformity in color across Ryugu's surface supports partial dehydration due to internal heating of the asteroid's parent body.

The asteroid 162173 Ryugu is the target of the Japan Aerospace Exploration Agency's (JAXA's) Hayabusa2 mission, which arrived in June 2018. Small asteroids, such as Ryugu, are thought to have been born from much older parent bodies through catastrophic disruption and reaccumulation of fragments during evolution of the Solar System (*1*, *2*). We seek to understand the properties of both Ryugu and its parent body. Deciphering the geologic record of an asteroid requires identification and characterization of the geological features on its surface. Detailed global observations of Ryugu were conducted with Hayabusa2's remote-sensing instruments, including the optical navigation cameras (ONCs), one of which is the nadir-viewing telescopic camera (ONC-T), with seven narrow-band filters [0.40 μm (ul), 0.48 μm (b), 0.55 μm (v), 0.59 μm (Na), 0.70 μm (w), 0.86 μm (x), and 0.95 μm (p)] (*3*–*5*); a laser altimeter [light detection and ranging (LIDAR) altimeter] (*6*); and a thermal infrared camera (TIR) (*7*), sensitive to wavelengths from 8 to 12 μm (*8*).

Global images were obtained from the home position located 20 km above the asteroid (*9*), from which we constructed a 0.55-μm map of Ryugu (Fig. 1A). Major geomorphologic features visible in this map include impact craters, boulders, troughs, and an equatorial ridge (Fig. 1B and table S3).

Impact craters

Impact crater morphologies, including rim and floor characteristics, provide indicators of surface age and mechanical properties. Approximately 30 circular depressions ≥20 m in diameter have been identified on Ryugu, many (at least half) with raised rims (Fig. 1A). Several craters also exhibit bowl-like shapes (Fig. 2, A and B), whereas others have shallow floors (fig. S10). The bowl-shaped depressions are classified on the basis of rim morphology and shape, providing confidence levels (CLs) to their identification as impact craters. CL1 features are circular with a clearly identifiable rim, CL2 depressions are circular but exhibit no rim, CL3 depressions are quasi-circular, and CL4 features are circular patterns of boulders with no clear topography. CL1 and CL2 depressions are most likely impact craters. The group of CL3 and CL4 features may include a few craters. Different levels of confidence are used in the statistical analyses to examine the robustness of the results. Laser-altimeter measurements indicate that fresh bowl-shaped depressions have depth/diameter ratios ranging from 0.14 to 0.2 (Fig. 2, C and D) (*8*). Although recent numerical calculations (*10*) show that large cavities may be formed in fast-spinning asteroids via the release of large boulders due to centrifugal force, raised rims are not expected to be generated in such a process. Thus, large equatorial craters on Ryugu are unlikely to have been formed by asteroid spin and are most likely of impact origin.

Some craters show evidence for motion of a loosely consolidated mass of materials on the

[1]The University of Tokyo, Tokyo 113-0033, Japan. [2]Planetary Exploration Research Center, Chiba Institute of Technology, Narashino 275-0016, Japan. [3]Kochi University, Kochi 780-8520, Japan. [4]Nagoya University, Nagoya 464-8601, Japan. [5]Rikkyo University, Tokyo 171-8501, Japan. [6]Institute of Space and Astronautical Science (ISAS), Japan Aerospace Exploration Agency (JAXA), Sagamihara 252-5210, Japan. [7]University of Aizu, Aizu-Wakamatsu 965-8580, Japan. [8]National Institute of Advanced Industrial Science and Technology, Tokyo 135-0064 Japan. [9]Kobe University, Kobe 657-8501, Japan. [10]Meiji University, Kawasaki 214-8571, Japan. [11]National Astronomical Observatory of Japan, Mitaka 181-8588, Japan. [12]SOKENDAI (The Graduate University for Advanced Studies), Hayama 240-0193, Japan. [13]Planetary Science Institute, Tucson, AZ 85719, USA. [14]Auburn University, Auburn, AL 36849, USA. [15]Tohoku University, Sendai 980-8578, Japan. [16]Brown University, Providence, RI 02912, USA. [17]Kindai University, Higashi-Hiroshima 739-2116, Japan. [18]Université Côte d'Azur, Observatoire de la Côte d'Azur, Centre National de le Recherche Scientifique (CNRS), Laboratoire Lagrange, 06304 Nice, France. [19]University of Arizona, Tucson, AZ 85705, USA. [20]Johns Hopkins University Applied Physics Laboratory, Laurel, MD 20723, USA. [21]German Aerospace Center (DLR), Institute of Planetary Research, 12489 Berlin, Germany. [22]International Research School of Planetary Sciences, Università d'Annunzio, 65127 Pescara, Italy. [23]Ashikaga University, Ashikaga 326-8558, Japan. [24]Hokkaido University of Education, Asahikawa 070-8621, Japan. [25]Max-Planck-Institut für Extraterrestrische Physik, 85748 Garching, Germany. [26]University of Stirling, FK9 4LA, Scotland, UK. [27]Research and Development Directorate, JAXA, Sagamihara 252-5210, Japan. [28]Nihon University, Funabashi 274-8501, Japan. [29]Osaka University, Toyonaka 560-0043, Japan. [30]Hitotsubashi University, Tokyo 186-8601, Japan. [31]Hiroshima University, Higashi-Hiroshima 739-8526, Japan. [32]Seoul National University, Seoul 08826, Korea. [33]NASA Johnson Space Center, Houston, TX 77058, USA. [34]Laboratoire d'Etudes Spatiales et d'Instrumentation en Astrophysique (LESIA)–Observatoire de Paris, Paris Sciences et Lettres (PSL), Centre National de le Recherche Scientifique (CNRS), Sorbonne Université, Université Paris-Diderot, 92195 Meudon Principal Cedex, France.
***Corresponding author: Email: sugita@eps.s.u-tokyo.ac.jp** †Deceased. ‡Present address: National Institute for Environmental Studies, Tsukuba 305-8506, Japan. §Present address: Mitsubishi Electric Corporation, Kamakura 247-8520, Japan.

inner walls (i.e., wall slumping; Fig. 2A). This phenomenon was not observed on another sub-kilometer asteroid, Itokawa (*11*), and indicates the presence of an unconsolidated surface layer. No crater has been found to have a floor with terrace structure, which would form if there was a large strength contrast between the surface and near-surface interior (*12*). These floor morphologies and the high fraction of raised rims indicate that the craters formed in an unconsolidated target, not dominated by pristine mechanical strength of the constituent surface material. Therefore, both gravity and weak cohesion strength controlled the crater formation. The individual boulders in the surface

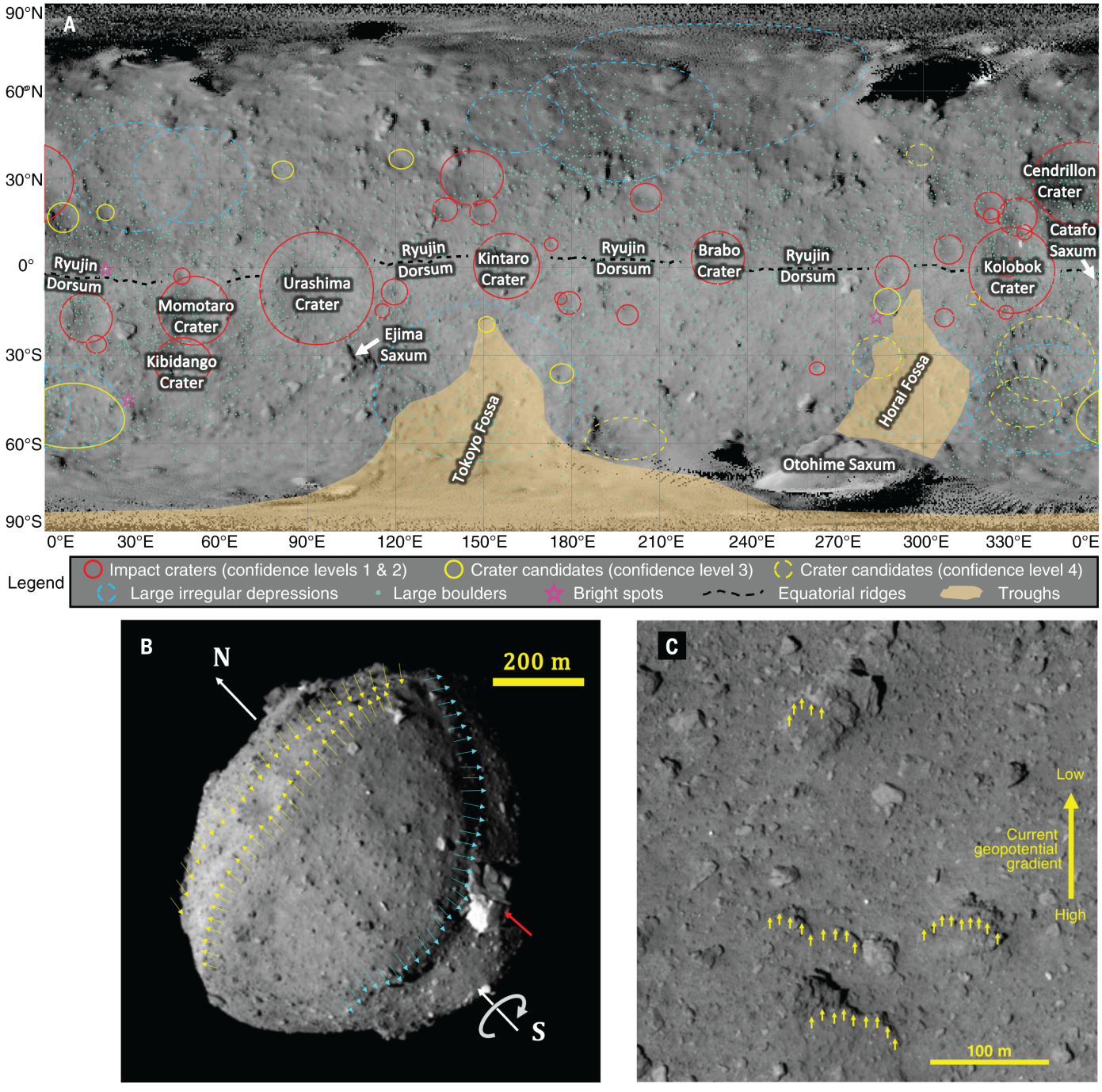

Fig. 1. Global map and images of Ryugu. (**A**) Geologic map of Ryugu based on mosaicked v-band (0.55 μm) images. Impact craters and crater candidates are indicated with circles, color coded by confidence level (see text). There is greater latitudinal exaggeration of map-projected surface area on Ryugu than for a sphere, because of its diamond-like cross section. This leads to the apparent higher crater number density in the equatorial region of this map. (**B**) Oblique view of Ryugu (image hyb2_onc_20180824_102748_tvf_l2b), showing the circum-equatorial ridge (yellow arrows), trough (blue arrows) extending from the equatorial region through the south polar region to the other side of Ryugu, and the large and bright Otohime Saxum (red arrow) near the south pole. The location of the poles and the spin direction are indicated with white arrows. (**C**) Asymmetric regolith deposits on imbricated flat boulders on the northern slope of the circum-equatorial ridge of Ryugu (hyb2_onc_20181003_222509_tvf_l2b). Small yellow arrows at the edges of regolith deposits indicate the direction of mass wasting. The large yellow arrow indicates the current geopotential gradient from high to low (*17*). The direction of geopotential gradient is consistent with the mass wasting.

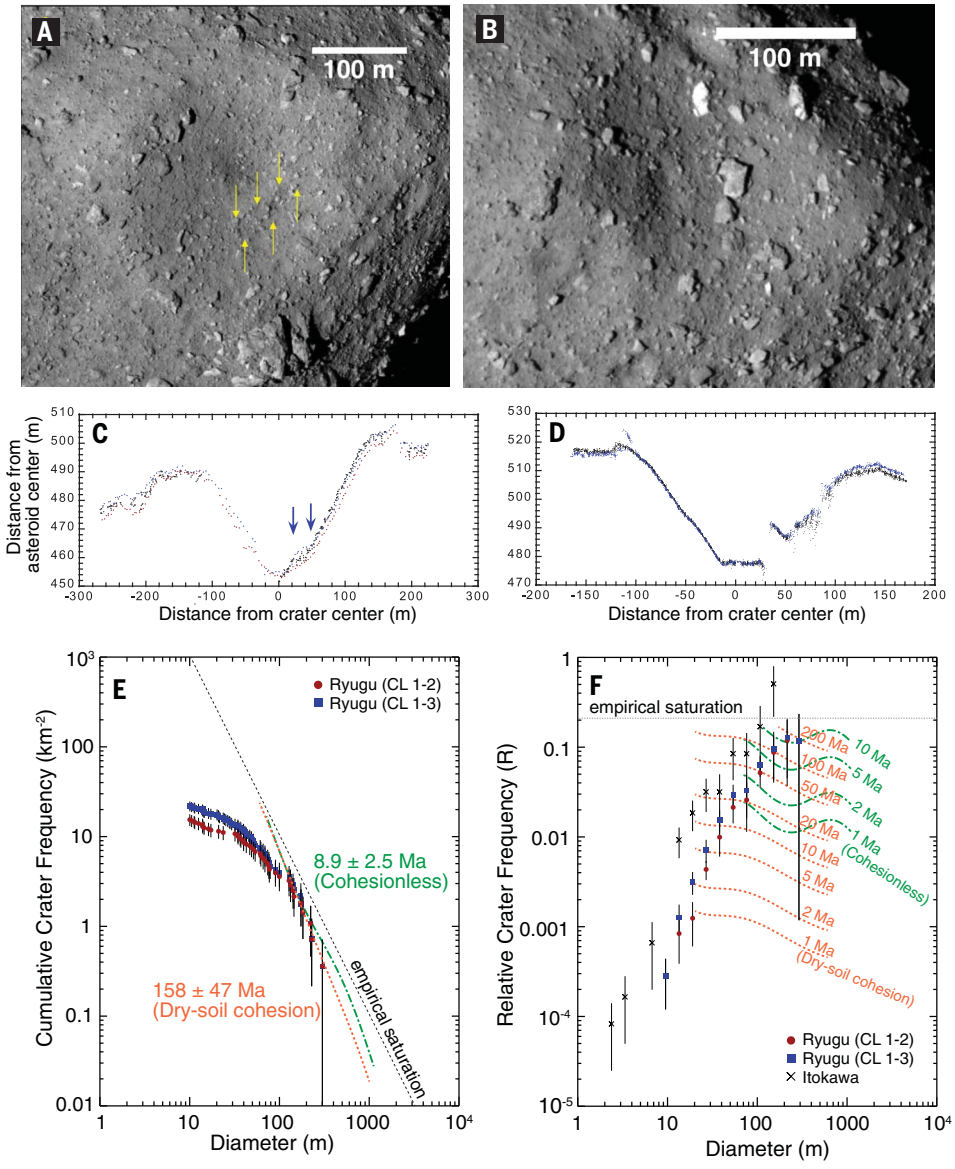

Fig. 2. Craters on Ryugu. (**A**) The largest crater, Urashima (290 m in diameter, 8.3°S, 92.5°E), on Ryugu (hyb2_onc_20180720_071230_tvf_l2b). Wall slumping is indicated with yellow arrows. (**B**) Kolobok crater (240 m, 1.5°S, 333.5°E), which has a deep floor, bowl-like shape, and a raised rim (hyb2_onc_20180720_100057_tvf_l2b). (**C**) LIDAR profiles of Urashima crater. Wall slumping is indicated with blue arrows. (**D**) LIDAR profiles of Kolobok crater. (**E**) CSFD on Ryugu and Itokawa and empirical saturation and crater production curves (*54*) with (orange) and without (green) dry-soil cohesion. Black crosses in (F) represent Itokawa crater candidates (*11*). Red and blue points indicate Ryugu craters with different crater CLs. (**F**) An R-plot (the CSFD normalized by D^{-2}, where D is diameter) for Ryugu (circles and squares) and Itokawa (crosses). The relative crater frequency R is defined as the differential crater frequency in a diameter range between D/k and kD, divided by D^3, where k is $2^{1/4}$. Saturation and crater production curves are the same as in (E). Ma, million years.

layer are large (~3 m in diameter) and are similar to the sizes of the projectiles (~0.1 to 1 m) that formed craters (~1 to 30 m) on Ryugu (*8*). Therefore, these large boulders may reduce crater size via armoring, in which a large fraction of impact energy is lost into the crushing or cratering of the first-contact boulder instead of forming a granular crater on the asteroid (*13*). Impact experiments using targets with constituent boulder sizes similar to the projectile's size indicate that armoring effects influence crater size and that a scaling relation for such targets must include a term for the breakup energy of the first-contact target boulder (*14*).

We estimated the surface crater retention age on the basis of the number density of craters 100 to 200 m in diameter, using a scaling rule with armoring effect (*14*), both with and without a dry-soil cohesion factor, obtaining surface ages of 10^8 and 10^7 years, respectively (Fig. 2E) (*8*). This large (i.e., a factor of 10) uncertainty in surface age comes from the influence of a small amount of cohesion, which controls the excavation flow near the crater rim. On a high-gravity planet, such as Earth, small cohesive forces do not influence crater size, but on microgravity bodies, such as Ryugu, crater size is influenced by the presence or absence of small cohesive forces, which is difficult to simulate in laboratory experiments on Earth. Despite these uncertainties, the observed crater size-frequency distribution (CSFD) indicates that the surface age of Ryugu is equal to or younger than the collisional lifetime (the mean time for an asteroid to experience a collision-induced catastrophic disruption) of kilometer-sized objects in the main asteroid belt [(3 to 5) × 10^8 years (*1*, *2*)] and equal to or older than the expected time (~4 × 10^7 years) Ryugu has stayed in a near-Earth orbit (*9*). Different collision frequencies must be considered for different scales of surface ages, because Ryugu is thought to have migrated from the main belt to its current near-Earth orbit, most likely through ν_6, the innermost resonance zone of the main belt (*9*, *15*). Because the collision frequency is far greater in the main belt, the majority of the craters ≥100 m probably formed while Ryugu was still resident in the main asteroid belt.

Ryugu's CSFD shows a dearth of small craters (<100 m; Fig. 2F). The deficit of small craters on Ryugu as a function of crater size is similar to that found for both Itokawa and Eros (*16*). Because craters in this size range on Ryugu are not greatly influenced by crater size reduction [owing to armoring effects (*14*)], these depletion patterns are more likely to be due to crater erasure processes, such as seismic shaking (*16*). The reduced number of small craters (<100 m) indicates that the crater retention time in this size range is very brief. The number density of craters ~10 m indicates that the average resurfacing of the top ~1-meter layer on Ryugu is <10^6 years for the main-belt impact flux (Fig. 2F) and <2 × 10^6 years

for near-Earth impact flux (fig. S3). Because impact cratering is a stochastic process, some of these small craters must have formed more recently, exposing fresh material.

Mass wasting

There is abundant evidence for mass movement along slopes (i.e., mass wasting) on Ryugu, particularly around the equatorial ridge and several craters, such as Urashima crater (Fig. 2A). Some groups of boulders observed along the equatorial ridge overlap one another with preferred orientations (i.e., imbrication) away from the ridge, and they are accompanied by asymmetrically distributed fragmental debris deposits (i.e., regolith). The edges of these boulders display little to no regolith deposits along the downhill sides of the ridge (Fig. 1C). Such imbrication typically occurs during landslides. The asymmetric regolith deposits along these boulders indicate that the direction of recent mass wasting is from the top of the equatorial ridge toward higher latitudes, consistent with Ryugu's current geopotential (*9*, *17*). Wall slumping is observed along crater walls, as discussed above (e.g., Fig. 2A). Some craters, such as Momotaro (12.5°N, 51.9°E) near the equatorial ridge, exhibit a higher concentration of large boulders on their floors than on their rims and walls (fig. S8). Such preferential concentration of larger boulders in topographic lows also occurs as a result of mass wasting. These observations suggest that the equatorial ridge is made of mechanically unconsolidated materials and may have formed during a period of rapid spin (*17*), as material flowed toward an equatorial topographic low. An unconsolidated nature would have allowed Ryugu to reshape, perhaps in response to a change in spin rate. When Ryugu was established in its current geopotential configuration, the ridge experienced mass wasting as some of the unconsolidated materials flowed toward new topographic lows at higher latitudes. Furthermore, interior walls in large craters, such as Urashima, exhibit evidence for mass wasting, such as imbricated boulders and run-up deposits (fig. S8B). This indicates that mass wasting postdates these large craters, which must have formed after the equatorial ridge.

Disk-averaged color

During Hayabusa2's approach phase (before arrival and parking at the home position), a series of disk-averaged photometric observations were acquired in each of the seven ONC filters over 12 different rotational phases. We used these data to examine the accuracy of the radiometric calibrations of ONC-T for each filter. Global reflectance values from the ONC-T images based on preflight and in-flight calibrations (*3*–*5*) were compared with ground-based photometric and spectral observations at 0.55 μm (*18*). The results were consistent within the uncertainties, validating that ONC-T is appropriately calibrated over all filters (*5*, *8*).

The disk-averaged seven-band color measurements exhibit little variation (<0.5%) over the different rotational phases observed (Fig. 3A). The color properties are consistent with the classification of Ryugu as a Cb-type asteroid, on the basis of the Bus taxonomy (*19*). This spectral type establishes connections with potential main-belt asteroid families and Ruygu's parent body. Some ground-based spectral observations have suggested the presence of hydrated minerals, owing to spectral features observed at 0.7 μm and <0.55 μm (*20*–*22*). This would imply that Ryugu's parent body could be a Ch-Cgh asteroid, similar to those in the Erigone asteroid family (*23*). However, the ONC-T color observations rule out such a parent body, as do results from Hayabusa2's Near-Infrared Spectrometer (NIRS3), which show that Ryugu's globally averaged near-infrared spectrum does not have any strong OH absorption band signature around 2.8 μm; only a weak absorption band is seen at 2.72 μm (*24*).

The observed visible spectral type is close to that of the asteroids Eulalia and Polana, which are the parent bodies of C-complex asteroid families in the inner main belt (*25*). The asteroid Erigone has a different spectral type (Fig. 3A). Orbital dynamics calculations have shown that the most likely origin of Ryugu is either Eulalia or Polana (*15*). The collisional lifetime of Ryugu [(3 to 5) × 10^8 years] is similar to or less than the breakup time of these families [830^{+370}_{-150} million years and 1400 ± 150 million years for Eulalia and Polana, respectively (*15*)]. Ryugu might not be composed of material directly ejected from one of these large bodies but could be the product of more than one generation of disruption (see below).

The link between Ryugu and Cb asteroids in the inner main belt has implications for possible meteorite analogs. The fraction of Cb- to B-type asteroids in the main asteroid belt is high; fig. S6 indicates that about half of the C-complex asteroids in the main belt are of types Cb, B, and C, which do not display a clear 0.7-μm band. Their populations in the inner main belt, from which the largest fraction of near-Earth asteroids is derived (*2*), contain many large families, such as the Eulalia and Polana families, with these spectral characteristics (*23*). Therefore, the B-Cb-C population comprises a large fraction of the material reaching Earth as meteorites. There are two major candidates for Ryugu meteorite analogs with sufficiently low-albedo materials: thermally metamorphosed carbonaceous chondrites (CCs) (*26*, *27*), or interplanetary dust particles (IDPs). The latter consist of highly primitive material that has experienced no (or only weak) water-rock reaction to form hydrated silicates (*28*, *29*).

Albedo and reflectance

Using the point-source and whole-disk observations of Ryugu, we performed Hapke modeling to characterize the disk-integrated photometric phase behavior in all seven ONC-T filters (table S1) (*8*). On the basis of these photometric measurements, we derived a geometric albedo of 4.5 ± 0.2% at 0.55 μm, similar to albedos of typical comets (*30*) and the darkest asteroids, such as 253 Mathilde, another Cb-type asteroid (*19*, *31*). We derived the disk-integrated surface reflectance at the standard laboratory observation angles (*i*, *e*, α = 30°, 0°, 30°; where *i*, *e*, and α are incident, emission, and solar phase angles, respectively) for comparison with meteorite samples measured in the laboratory.

The average value of the standard-condition reflectance factor is 1.88 ± 0.17% at 0.55 μm, which is lower than that of any meteorites reported in the literature. The darkest meteorite samples described in the published literature are the thermally metamorphosed CCs (*26*, *32*). Recent measurements show that meteorites of this type (e.g., Jbilet Winselwan, Y-86029, and Y-793321) exhibit reflectance similar to that of Ryugu (Fig. 3B). These meteorite samples are classified in the weakly heated and moderately heated groups (stages II and III, respectively), in which hydrated silicates have been altered into amorphous silicates as a result of dehydration but have not recrystallized into olivine or pyroxene (*33*). Most of these samples are powders; rough slab surfaces, such as Ryugu's surface, generally exhibit lower reflectance and bluer spectra. Although spectral data for slab samples are not as frequently reported as data for powder samples, slab spectra of major CCs from each clan, such as Murchison and Mighei for CM and Ivuna for CI, have been measured (*34*, *35*). These slab samples are not consistent with Ryugu's spectrum.

Local color variation and age–color relation

Surface colors at specific locations on Ryugu span a large range, and all are consistent with the colors of C-complex asteroids (Fig. 3). The color of the majority of Ryugu's surface is characteristic of regolith (denoted "typical regolith"; Fig. 3, C and D). Other colors are found in relatively limited areas and/or geological features on Ryugu, such as distinctive boulders and crater bottoms. Thus, we analyze the color of all pixels on Ryugu with small incidence and emission angles ($i \leq 40°$ and $e \leq 40°$) and use them to define the regolith color variation across the surface.

The general spectral slope from b-band (0.48 μm) to x-band (0.86 μm) exhibits the greatest regional variation; Ryugu's surface has bluer spectral slopes at both poles, on the equatorial ridge, and in large troughs (Fig. 3E). Both polar regions and the equatorial ridge are topographic highs, which may be subject to gradual erosion, leading to the exposure of fresh surface material. Steep boulder surfaces, which may have recently experienced erosion due to thermal fatigue (*36*) or other processes, tend to have brighter and bluer surfaces (Fig. 3, C and D). In contrast, many locations conducive to deposition, such as crater floors, exhibit redder and darker colors. These observations suggest that exposure of Ryugu materials to space leads to their reddening and darkening. However, it is not clear whether this trend occurs because of space weathering or other processes, such as coating with redder and darker dust (*8*). Local-scale heterogeneity suggests that the large-scale uniformity may not be due to pristine materials on

Ryugu's surface, but instead may be the result of a well-mixed surface.

No regolith-covered surface on Ryugu exhibits a strong 0.7-μm absorption in the ONC-T color data. Dynamical calculations have shown that many near-Earth objects (NEOs) experienced dehydration during orbital excursions near the Sun, which may have contributed to the depletion in 0.7-μm absorption in C-complex NEOs (*37*). NEOs with Ryugu-like orbits may experience large orbital excursions on a time scale of 10^7 years, and the skin depth of solar heating during Ryugu's orbital evolution is tens of centimeters (*9*). This time scale is longer than the retention age (<2 × 10^6 years) of 10-m craters,

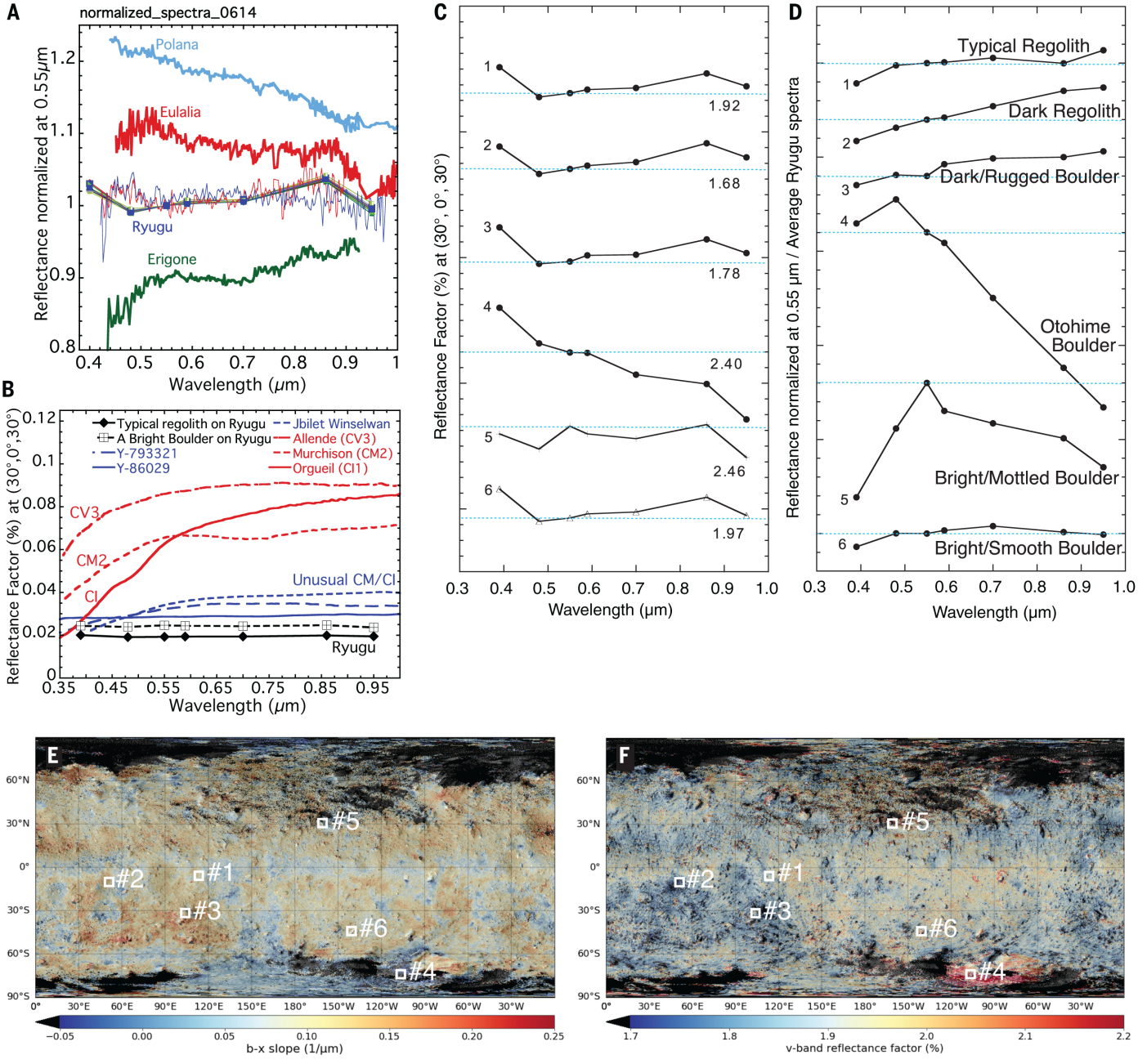

Fig. 3. Multiband colors of Ryugu's surface. (**A**) Comparison between disk-averaged spectra (lines with squares, normalized at 0.55 μm) for Ryugu at 12 different rotational phases and ground-based observations (lines without symbols) of Ryugu from (*55*) (blue) and from (*21*) (red). Data are also shown for the large main-belt asteroids Polana, Eulalia, and Erigone (*56*), each of which is the parent body of an asteroid family. Because of the similarity among the spectra taken at different phases, individual lines for Ryugu overlap. Spectra are offset by 0.1 for clarity. (**B**) Comparison between typical Ryugu surface colors (black) (reflectance factor at 30°, 0°, 30°) and those of dehydrated CCs (blue) and typical CCs (red). Individual meteorite names are indicated. The spectrum of a powder sample (≤155 μm) of Jbilet Winselwan was measured at 30°, 0°, 30° with the spectrometer system at Tohoku University (*57*). The rest of meteorite spectra are from (*58*). (**C**) Reflectance spectra of typical morphologic and color features on Ryugu. Locations of features (labeled 1 to 6) are shown in (E) and (F) and in fig. S12. Individual spectra are shifted vertically for clarity. Vertical-axis tick spacing is 0.05%. (**D**) Same as (C), but normalized by the Ryugu average spectrum. Vertical-axis tick spacing is 0.01. (**E**) b-x slope map (inverse micrometers) and (**F**) v-band reflectance factor map (percent) superposed on a v-band image map. The equatorial ridge and the western side (160°E to 290°E) have slightly higher v-band reflectances than other regions (see fig. S13 for statistical analysis).

which excavate unheated substrate material (crater depths ~1 m). Thus, the lack of a high degree of hydration on Ryugu is unlikely to be due to solar heating during a recent orbital excursion.

East-west dichotomy

Ryugu's western side (160°E to 290°E), which is surrounded by troughs (Fig. 1, A and B), has a v-band albedo higher than that of other areas (Fig. 3F and fig. S13). This western side also has a lower number density of large boulders (Fig. 4A). The topographic highs and bluish b-x spectral slope of the equatorial ridge transect the troughs, suggesting that the equatorial ridge formed more recently than the troughs. Although the equatorial ridge has depressions around 160°E and 290°E, the morphologic characteristics of these features are more consistent with those of impact craters, so we do not consider them to be connected to the mass motion that formed the trough. The formation of the east-west dichotomy probably predates the equatorial ridge formation. However, because there is no difference in b-x spectral slope between the western side and other regions on Ryugu, the nature of its enhanced reflectance is probably not the result of a shorter exposure to the space environment. In contrast, the coincidence between high v-band reflectance and low boulder abundance suggests that this dichotomy may reflect smaller grain size in the western hemisphere. The two hemispheres may have different physical properties, such as grain size and mobility, which could be the result of reaccumulation of two large rubble piles with different grain sizes during the reaccumulation stage immediately after the catastrophic disruption of the parent body (see the "Implications for the evolution of Ryugu's parent body" section below).

Principal components analysis

We conducted a principal components analysis (PCA) of the ONC-T filter data and the second phase of the Small Main-Belt Asteroid Spectroscopic Survey (SMASSII) observations of C-complex main-belt asteroids by ground-based telescopes. This method has been used widely for asteroid spectral analysis and has served as a basis for spectral type definitions (*19*, *38*). Because most reflectance data registered in SMASSII covers only 0.43 to 0.9 μm, we limited the ONC-T data to the b to x bands, excluding the ul and p bands centered at 0.39 and 0.95 μm. Because PCA can expand spectra into orthogonal basis functions, PCA often extracts linear combinations of spectra with physical or mineralogic meanings as the principal components (PCs). Nonorthogonal linear combinations of the second and third PCs produced by our analysis (PC2 and PC3) correspond to the 0.7-μm absorption and drop-off in reflectance shortward of v-band (Fig. 5B and fig. S5). Our results indicate that regolith spectra from ONC-T are consistent with moderately dehydrated CCs (e.g., Y-86029) and reside both near the edge of the B-Cb-C population and the dehydration tracks for CM and CI chondrites (Fig. 5B and fig. S4).

TIR observations provide constraints on surface grain size, which influences the PCA results of colors on Ryugu. TIR observations indicate that the peak temperatures of Ryugu's surface correspond to uniform thermal inertia values between 200 and 500 J m^{-2} $s^{-0.5}$ K^{-1} (Fig. 6). These values are consistent with the disk-averaged value (150 to 300 J m^{-2} $s^{-0.5}$ K^{-1}) estimated on the basis of prearrival telescope observations (*39*) and suggest subcentimeter to 10-cm grains (*7*, *40*); the fraction of surface area covered with grains ≤1 mm

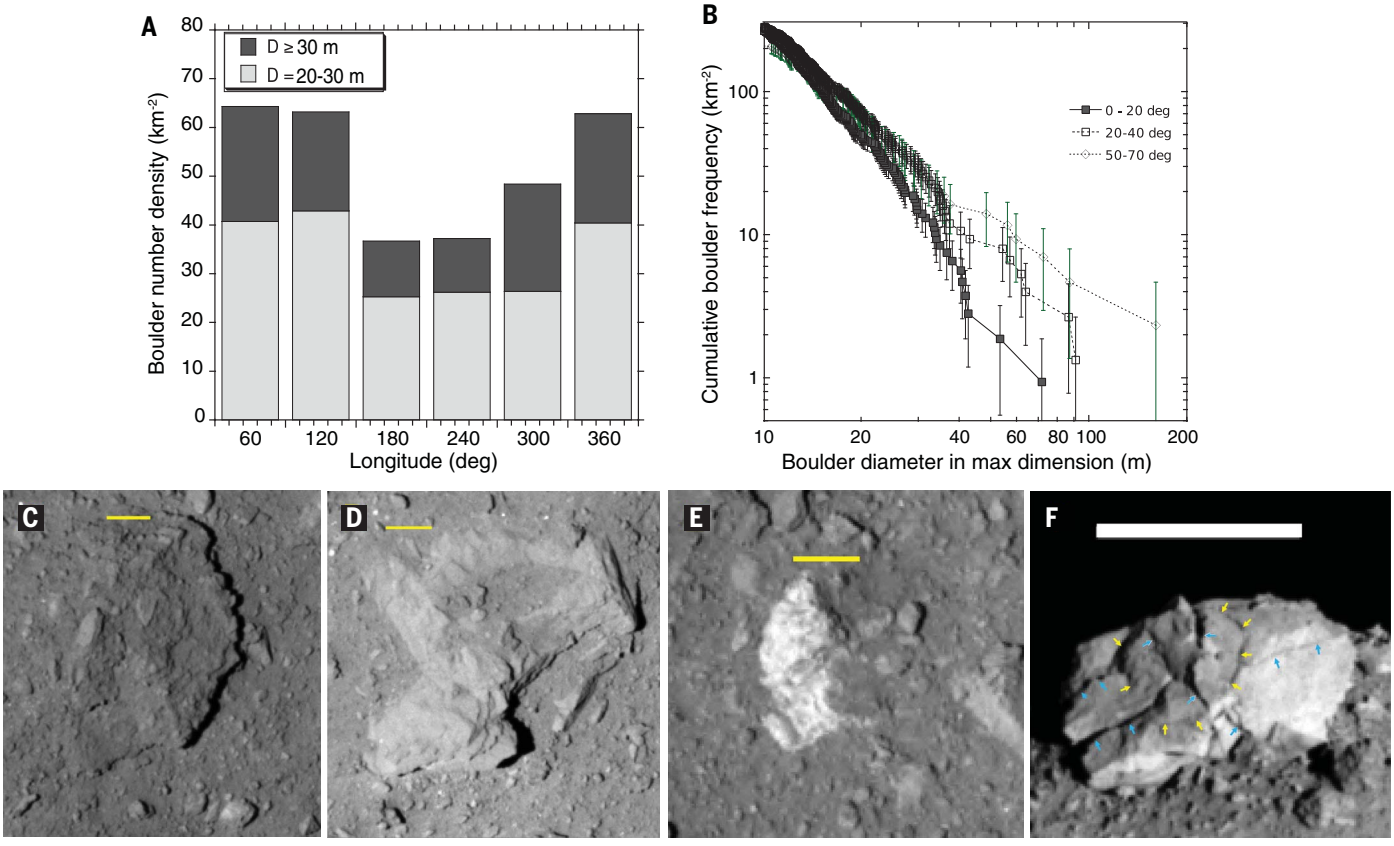

Fig. 4. Statistics and morphologies of boulders on Ryugu. (**A**) Distribution in longitude of boulders with diameters of 20 to 30 m and ≥30 m. (**B**) Cumulative size distribution of large boulders, compared between different latitudinal zones. (**C**) A type 1 boulder, which is dark and rugged (hyb2_onc_20181004_042509_tvf_l2b). A close-up view of its layered structure is shown in fig. S11D. (**D**) A type 2 bright boulder with smooth surfaces and thin layered structure (hyb2_onc_20181004_012509_tvf_l2b). A close-up view of its layered structure is shown in fig. S11E. (**E**) A type 3 bright and mottled boulder (hyb2_onc_20180801_213221_tvf_l2b). (**F**) The sole type 4 boulder, Otohime Saxum, has concentric (yellow arrows) and radial (blue arrows) fractures, consistent with a fracture system generated by an impact (hyb2_onc_20180719_124256_tvf_l2b). In (C) to (F), the brightness of each image is stretched independently. The yellow and white scale bars are 10 and 100 m, respectively.

is very small. Laboratory examination of CC powders of different grain sizes demonstrates that in the visible wavelengths the reflectance and spectral slope do not change markedly for grain sizes larger than ~1 mm, although the effects of compaction and thin coating of fine powers may influence the spectra (*41*). Comparison between the PCA results of Ryugu's surface and the dehydration track for heated coarse-grained samples of the Murchison meteorite shows that the distribution of Ryugu's surface is much narrower than that of the Murchison dehydration track in the PC space (Fig. 5B), suggesting that Ryugu is dominated by materials that experienced similar degrees of dehydration.

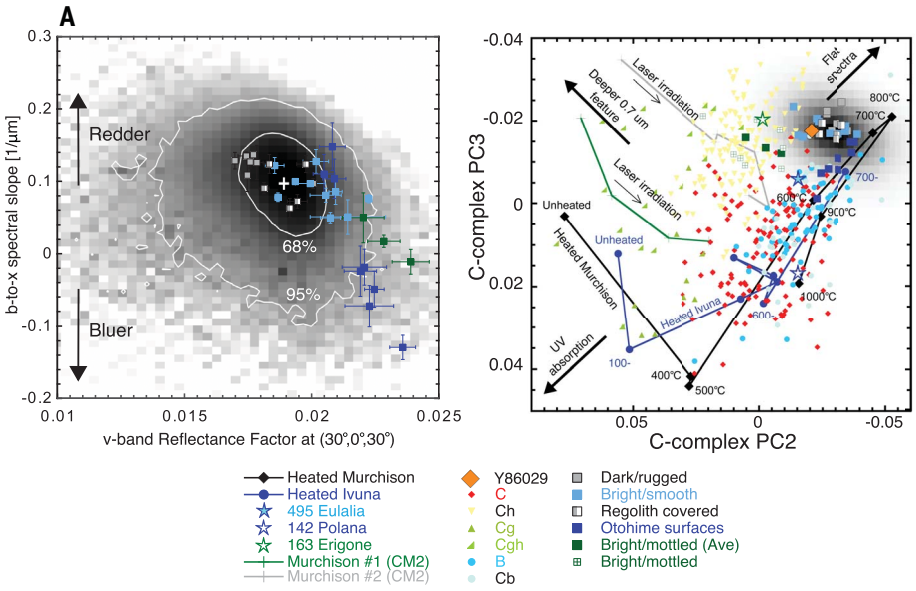

Fig. 5. Colors of surface features on Ryugu. Colors measured from ONC-T images are compared between areas of regolith (gray-black contour) and the four types of boulders (solid, monotone squares) on Ryugu. The legend applies to both panels. (**A**) Comparison of v-reflectance factor and b-x slope distribution. The average value of Ryugu's surface is indicated with a white cross. Contours indicate 95 and 68% of the surface area. (**B**) Comparison of principal component space (PC2-PC3) and main-belt C-complex asteroids (*56*) (colored circles), a moderately dehydrated CC [Y-86029, orange diamond (*58*)], Murchison (CM2) samples with heating [black line (*58*)] and laser irradiation [light green (*59*) and gray lines (*58*)], and heated Ivuna (CI) samples [blue line (*58*)]. Parent bodies of major asteroid families in the inner main belt, Polana (open blue star), Eulalia (solid light blue star), and Erigone (open green star), are also shown (*56*). Images of the four types of boulders are shown in Fig. 4 and fig. S11. Thick black arrows denote locations of end-member spectra (spectra with deep 0.7-μm absorption, flat spectra, and spectra with deep ultraviolet absorption) in this PC space.

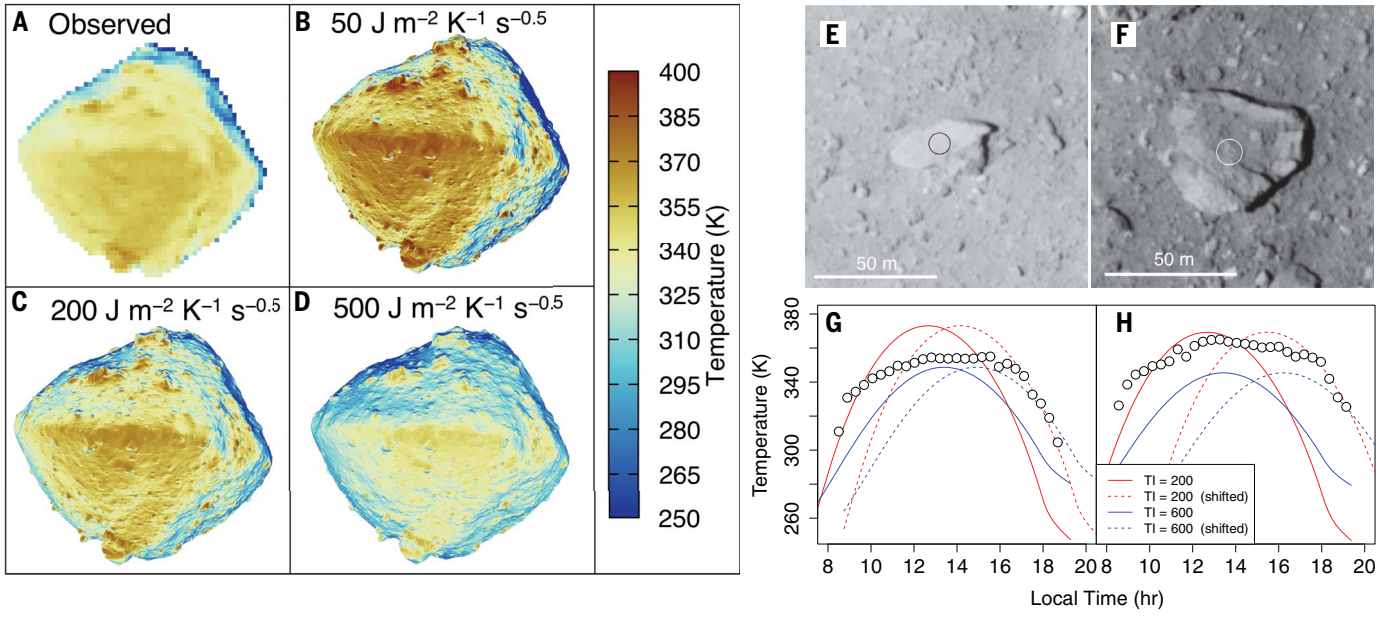

Fig. 6. Thermal infrared camera measurement results. (**A**) Brightness temperature image taken with TIR at 06:07:11 UTC on 10 July 2018 (hyb2_tir_20180710_060711_l2). (**B** to **D**) The image in (A) compared with calculated thermal images by using the structure-from-motion shape model (*17*), assuming uniform thermal inertia of (B) 50, (C) 200, and (D) 500 J m^{-2} $s^{-0.5}$ K^{-1}, respectively. (**E**) An ONC-T image of large boulders (6.4°S, 148.4°E), taken during low-altitude (5 to 7 km) observations (hyb2_onc_20180801_144909_tvf_l2b). Surface area (open circle) not covered with regolith was chosen for temperature analysis. (**F**) As in (E), but for a boulder at (20.9°S, 27.8°E) (hyb2_onc_20180801_174157_tvf_l2b). (**G**) Temperature profile of the location indicated with the circle in (E) observed with TIR at 20 km from the Ryugu center (open circles). Theoretical temperature profiles for uniform thermal inertias of 200 and 600 J m^{-2} K^{-1} $s^{-0.5}$ are shown with curves. Solid curves are for a horizonal plane that starts to receive solar light at local time 7.5 hours; dashed curves represent a tilted plane that receives sunlight at later times. The observed data are largely enclosed by the upper envelopes of time-shifted curves for 200 and 600 J m^{-2} K^{-1} $s^{-0.5}$. (**H**) Same as (G), but for the location indicated by the circle in (F).

Abundance and distribution of boulders

Ryugu's surface contains many boulders that span a wide range of sizes (Fig. 4B). The largest boulders (>20 m) are too large to be ejecta from the observed craters (≤300 m) (*42*), which suggests that they are instead fragments of Ryugu's parent body. The cumulative distribution of boulder sizes follows a power law with an exponent between −2.5 and −3 (Fig. 4B), similar to that measured for other small asteroids (*43*–*45*).

The global average number density of boulders ≥20 m in diameter at latitudes ≤70° is 50 km^{-2} on Ryugu, which exceeds the value for Itokawa by a factor of 2 (*39*, *41*). However, the number density of craters on Ryugu is of the same order of magnitude as that of Itokawa, which suggests that boulders on both asteroids have experienced similar degrees of meteoritic bombardment. Thus, the higher abundance of large boulders on Ryugu suggests that the impact strength of these boulders may be of a similar order of magnitude to that of Itokawa's boulders. Given the apparent high surface mobility, it is possible that many previously existing boulders may have been ejected from Ryugu as macroscopic bodies. If so, fragments from Ryugu may reach Earth as macroscopic meteorites.

The spatial distribution of boulders on Ryugu differs from that on Itokawa and Eros, which have boulder-poor regions, such as smooth terrains (*46*, *47*) and regolith ponds (*48*). Ryugu does not contain large areas with low boulder abundance, suggesting that the degree of size sorting is much lower on Ryugu. A contributing factor may be the difference in the overall shape of these asteroids: Itokawa and Eros are elongated, whereas Ryugu is spheroidal. However, there is evidence for some global size segregation in the latitudinal variation in boulder size: The boulder number density is lower in the equatorial region than at higher latitudes (Fig. 3A). This may be because of mass flow during the equatorial ridge formation (*17*). There is also a smaller boulder abundance variation in the longitudinal direction (Fig. 3B), with the boulder abundance in the western hemisphere (160°E to 290°E) systematically lower than at all other longitudes on Ryugu.

Color and morphology of boulders

There is a systematic trend between boulder colors and morphologies on Ryugu. We have identified four distinct morphologic boulder types. (i) Type 1: Dark and rugged boulders. This type possesses rugged surfaces and edges, tends to have uneven layered structures possibly related to inclusion of coarse-grained clasts (Figs. 4C and fig. S11A), and has color properties similar to Ryugu's average color (Fig. 3C). Many boulders of this type are partially buried by regolith; as is the case for Ejima Saxum (Fig. 1A). (ii) Type 2: Bright and smooth boulders. This boulder type displays several thin and parallel layers (Fig. 4D). Many of these boulders are positioned atop the regolith, and some exhibit distinctive striped patterns (fig. S11B). Their typical color ranges from slightly bluer than average to Ryugu's average color (Fig. 3). (ii) Type 3: Bright and mottled boulders. This boulder type does not show clear layers but displays a blocky variegation in albedo (Fig. 4E and fig. S11C). The bright parts exhibit a drop-off in reflectance at short wavelengths (ul and b) (Fig. 3C). (iv) Type 4: The largest boulder on Ryugu, Otohime Saxum, does not match the other types. It is located near the south pole (Figs. 1 and 4F), with sharp edges and smooth surfaces but no obvious layering. Its vertical face is the brightest surface on Ryugu and exhibits a very blue color (Fig. 3). The differences in brightness among these four types of boulders are not very large; the range of their v-band reflectance factors is similar to that of the background regolith (Fig. 5A).

More quantitative examinations of boulder colors were performed using reflectance-slope statistics and PCA. Although the dark, rugged boulders and the bright, smooth boulders are distinct in morphology, they form a single linear trend in reflectance-slope diagrams and PC2-PC3 space (Fig. 5) parallel to the general distribution of PC scores over the entire surface. The range in boulder color variation is similar to the color variation seen over the entire surface; the range of PC2 scores of 27 large boulders encompasses the PC2 score range of more than half of Ryugu's surface. This agreement in PC-score trends between regolith and boulders suggests that the color variation in regolith on Ryugu may be controlled by the color variation of these two types of boulders, from which the regolith may be produced through comminution processes.

In contrast, the different sides or facets of Otohime Saxum form their own trend in the reflectance-slope diagram (Fig. 5A) and PC spaces (Figs. 5B and fig. S7), approximately parallel to the trend for heat-induced dehydrated CC materials (*26*). The trend observed for Otohime Saxum is also parallel to the distribution trend in the B-Cb-C population (Fig. 5B and fig. S4), which suggests that their color variations may result from the same process, such as dehydration.

In the PC2-PC3 space, the bright, mottled boulders are consistent with the Ch-Cgh asteroid population, closest to Erigone (Fig. 5B). These type 3 boulders extend the trend seen in the regolith and other types of boulders (Fig. 5B and fig. S7). The 0.7-μm absorption—measured as the difference, $(v + x)/2w - 1$, between w-band reflectance and the linear continuum defined by v- and x-band reflectance values—is not stronger than the average Ryugu spectrum. Type 3 boulders are close in PC space to the Ch-Cgh population, owing to their low b-band reflectance.

The linear trend extending through type 3 boulders, the average regolith, and type 1 and 2 boulders is seen in the first three PC values plotted against albedo. This trend cannot be produced by space weathering and/or grain size effects. It also differs from the L-shaped distribution of laboratory dehydration data (Fig. 5B). Although the low-temperature evolution of the dehydration track for CM chondrites is similar to the boulder trend (both cross the dividing gap between Ch-Cgh and B-Cb-C populations and have a large PC2 change), they differ in PC3 change, leading to a very different slope in the PC2-PC3 space. Instead, the trend formed by boulder types 1 to 3 connects the average Ryugu spectrum and the Ch-Cgh population. A simple interpretation of these trends is the mixing between two components in Ch-Cgh and B-Cb-C populations. This trend is consistent with mixing seen not only in the regolith but also in the boulders. This observation based on PCA suggests that these boulders have experienced mixing processes.

Boulder texture and regolith grains

Hayabusa2 carried several landers [encompassed by three MIcro Nano Experimental Robot Vehicles for Asteroid (MINERVA-IIs) and the Mobile Asteroid Surface Scout (MASCOT)]. Deployment of these landers required multiple spacecraft descents to <100-m altitude, which provided opportunities for obtaining close-up images down to a scale of 6 mm per pixel (Fig. 7 and fig. S14).

The higher-resolution images show that the global size distribution of both boulders and pebbles follows a power-law distribution down to decimeter scales; the slope (i.e., power-law index) of their cumulative size distribution is about −2.5 at sizes larger than ~0.2 m, similar that found for large blocks (10 to 160 m) (Fig. 4B). The slope then becomes shallower at smaller sizes (fig. S14A). The shallower slope in the small size range suggests a non-negligible mechanical strength of individual boulders and pebbles on Ryugu. Although such high-resolution measurements have been conducted only in limited areas on Ryugu, no differences have been observed between areas on and off the equatorial ridge.

Many images of Ryugu exhibit bright spots (Fig. 7, A and B, and fig. S14B). Some of these spots are brighter than the average background by a few tens of percent, whereas others are brighter by a factor of 2 or greater. These spots may be impact craters or recent fragments from preexisting boulders, both of which could exhibit higher albedos because of the freshness of their interior, or they may be small fragments of distinct intrinsic composition. Their distinctive brightness and relatively low abundance suggest that they may be composed of materials similar to bright and mottled boulders, whose spectra are consistent with Ch-Cgh populations (Fig. 5). Ryugu's surface material may be a mixture of materials with different lithologies representative of its parent body.

Heterogeneity in brightness can also be found within individual boulders (Fig. 7A). This morphologic characteristic is consistent with coarse-grained clastic rocks (impact breccia), including rock fragments broken by impact. The majority constituent of CCs has been proposed to be impact breccia (*49*). This suggests material mixing before these boulders were formed, which likely took place on Ryugu's parent body. Because impact breccias can contain multiple components with variable mixing ratios, they can readily account for the mixing trends seen in the PC spaces (fig. S7). Breccia formation on the parent body

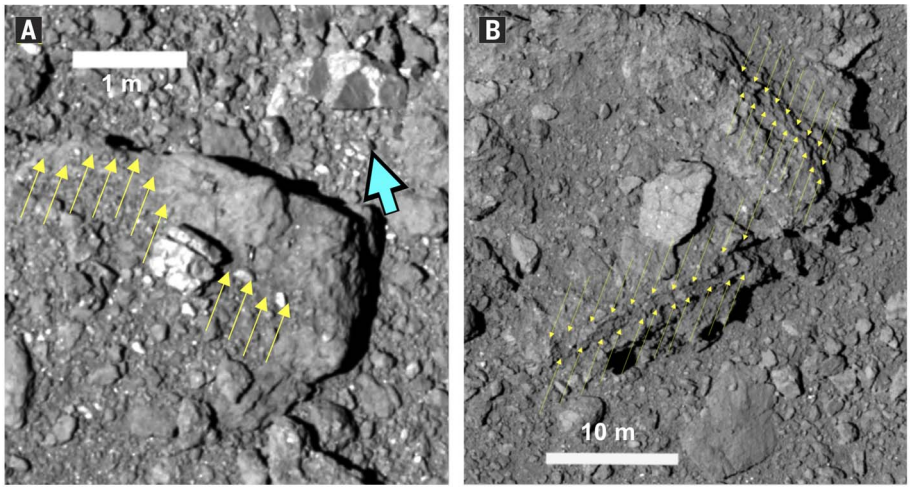

Fig. 7. Close-up observation results of surfaces on Ryugu. (**A**) A boulder partially buried with regolith (yellow arrows) and a smaller boulder with angular fragments having different brightness (blue arrow) near the MINERVA-II landing site (9 mm per pixel, hyb2_onc_20180921_040154_tvf_l2b). (**B**) A rugged boulder with layered structure (yellow arrows) near the MASCOT landing site (6 cm per pixel, hyb2_onc_20181003_003036_tvf_l2b).

can also account for porous textures observed in many dark boulders on Ryugu (Fig. 7B). These porous boulders seen in the high-resolution images have the same morphologies as the dark, rugged boulders observed in lower-resolution global and regional images (Fig. 4C). These boulders often have quasi-parallel layers (Fig. 7B). Thus, if these boulders are impact breccias, they may originate from the sedimentation of multiple ejecta blankets.

Layered structures are seen on boulder surfaces, suggesting that these boulders are not covered with loose regolith, supporting our interpretation that the thermal inertias of boulders measured by TIR (Fig. 6) reflect the bulk properties of the boulders. The presence of rugged grains and pores is also consistent with low thermal conductivity and density.

The porous nature of impact breccias would increase the bulk porosity of Ryugu. The very low bulk density [$(1.19 \pm 0.02) \times 10^3$ kg/m^3] of Ryugu would require very high porosity (~50%) if the grain densities of typical CCs are assumed (*17*). Such a high porosity is substantially greater than that (~40%) for closest packing with a single boulder size. If Ryugu possesses pores within individual boulders (intraboulder pores) in addition to pores between multiple boulders (interboulder pores), such low density can be achieved with typical CC materials.

Implications for the evolution of Ryugu's parent body

Our observations suggest the presence of partially hydrated minerals on Ryugu, though with a low degree of hydration. The low average albedo (Fig. 3B), average spectra lying in the midrange of dehydration tracks of CM and CI chondrites (Fig. 5B), and shortward drop-off in the spectra of some boulders (Fig. 3D) are consistent with moderately dehydrated CCs and/or weakly altered IDPs and are inconsistent with completely dehydrated CCs. In this section, we discuss the origin of these materials on Ryugu.

Recent numerical calculations of large asteroid breakups by collision show that fragments formed by the reaccumulation of material, resulting in a rubble pile structure, can contain materials sampling different depths on the original parent asteroid (~100 km in diameter) (*50*). Mixtures of impact debris with different lithologies from the original parent body could deposit on the reaccumulated fragments, leading to the formation of impact breccias. A subsequent impact on such a reaccumulated fragment would generate boulders with a large heterogeneity in color properties. Using a similar method, we conducted numerical calculations to estimate how much material is collected in reaccumulated bodies from different depths of a 100-km–diameter parent body (*8*) (fig. S9). The results indicate that materials from all depths of the parent body are accumulated in each small reaccumulated body. This could account for both the relatively homogeneous spectral properties of Ryugu and the limited amount of local heterogeneity found in the boulders, if partial dehydration occurred as a result of internal heating (e.g., due to radioactive decay of ^{26}Al). Internal heating can warm a large fraction of the volume of the parent body relatively uniformly, leaving a small volume of outer layer relatively cool (*51*) (Fig. 8).

In contrast, partial dehydration due to a single-shock heating event, such as that induced by the catastrophic impact that disrupted the original parent body, is unlikely because most boulders on Ryugu do not possess a strong 0.7-μm absorption band. To suppress the 0.7-μm band in the majority of a resulting body composed of reaccumulated fragments, the impact must heat the relevant mass to 400°C or higher. However, impact heating is an inefficient global process; efficient heating occurs only around the impact site (fig. S15). Most of the volume does not experience much heating and simply fractures into cold impact fragments. The numerical calculation results (*50*) (fig. S9) indicate that a catastrophic disruption event due to a large impact would sample different portions of the parent body along the excavation streamlines. Thus, any body formed from reaccumulated fragments would be primarily heterogeneous unless the parent body itself was homogeneous—i.e., the large-scale radial heterogeneity in the parent body would be inherited by the boulders comprising the reaccumulated-fragments body. Consequently, the preponderance of materials with little water signature on Ryugu suggests that a dominant part of its original parent body was also water poor. Such global partial dehydration is possible with impacts, but only if many impacts occurred before the catastrophic disruption (Fig. 8). Geochemical analyses of thermally metamorphosed meteorites are consistent with short-term heating (*27*, *52*); thus, this scenario cannot readily be discarded. However, the observation that Ryugu's regolith and boulders are concentrated in a relatively small area in the dehydration track in the PC spaces suggests that a large volume of Ryugu's original parent body was dehydrated to a similar state. Such uniformity is more consistent with internal heating on the parent body than partial dehydration caused by multiple impacts.

An alternative possibility is that Ryugu is covered with materials that experienced only incipient aqueous alteration before forming Fe-rich serpentine, which has 0.7-μm absorption. In this scenario, the closest meteoritic counterpart would be IDPs. If Ryugu is made of such highly primitive materials, the trend connecting regolith and dark boulders in the B-Cb-C population with bright, mottled boulders in the Ch-Cgh population may be a progression of aqueous alteration (*28*, *29*). However, there are insufficient IDP reflectance spectra available to constrain this scenario. It is difficult to distinguish materials that experienced only a low degree of hydration from materials that originally were highly hydrated and subsequently experienced partial dehydration. Nevertheless, the boulders on Ryugu have survived impact processes during catastrophic disruption, the reaccumulation process, and more-recent impacts on Ryugu; they are not dust balls with little cohesion. Thus, this scenario is in conflict with the boulder-rich nature of Ryugu. If Ryugu is composed of IDP-like materials and does not have a macroscopic meteorite counterpart, there must be an additional mechanism to break up boulders and pebbles before they arrive at Earth as meteorites.

Although multiple scenarios for the evolution of Ryugu's parent body remain viable, our comparison between Hayabusa2 remote-sensing data, meteoritic samples, and asteroids leads us to prefer the scenario of parent-body partial dehydration due to internal heating. This scenario suggests that asteroids that accreted materials that condensed at ≤150 K (the H_2O condensation

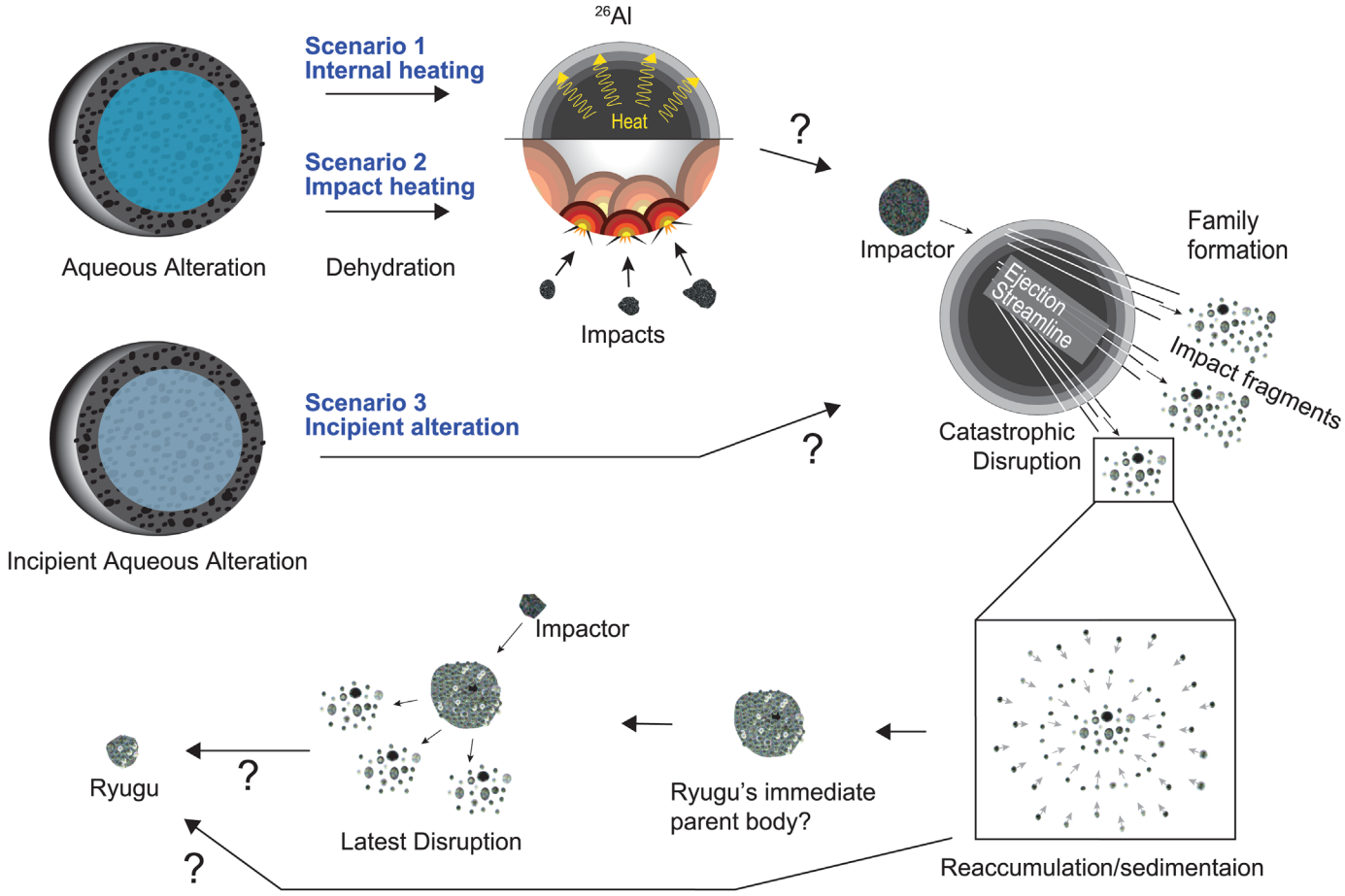

Fig. 8. Schematic illustration of Ryugu's formation. Ryugu formed from the reaccumulation of material ejected from an original parent body by an impact, possibly by way of an intermediate parent body (bottom). Three scenarios to explain Ryugu's low hydration and thermal processing may have occurred before disruption of the original parent body (top).

temperature under typical solar nebula conditions) must have either formed early enough to contain high concentrations of radiogenic species, such as ^{26}Al, or formed close to the Sun, where they experienced other heating mechanisms (*53*). The degree of internal heating would constrain the location and/or timing of the snow line (the dividing line between H_2O condensation and evaporation) in the early Solar System.

REFERENCES AND NOTES

1. D. P. O'Brien, R. Greenberg, The collisional and dynamical evolution of the main-belt and NEA size distributions. *Icarus* **178**, 179–212 (2005). doi: 10.1016/j.icarus.2005.04.001
2. W. F. Bottke Jr. *et al*., The fossilized size distribution of the main asteroid belt. *Icarus* **175**, 111–140 (2005). doi: 10.1016/j.icarus.2004.10.026
3. S. Kameda *et al*., Preflight calibration test results for optical navigation camera telescope (ONC-T) onboard the *Hayabusa2* spacecraft. *Space Sci. Rev.* **208**, 17–31 (2017). doi: 10.1007/s11214-015-0227-y
4. H. Suzuki *et al*., Initial inflight calibration for Hayabusa2 optical navigation camera (ONC) for science observations of asteroid Ryugu. *Icarus* **300**, 341–359 (2018). doi: 10.1016/j.icarus.2017.09.011
5. E. Tatsumi *et al*., Updated inflight calibration of Hayabusa2's Optical Navigation Camera (ONC) for scientific observations during the cruise phase. *Icarus* **325**, 153–195 (2019). doi: 10.1016/j.icarus.2019.01.015
6. T. Mizuno *et al*., Development of the laser altimeter (LIDAR) for Hayabusa2. *Space Sci. Rev.* **208**, 33–47 (2016). doi: 10.1007/s11214-015-0231-2
7. T. Okada *et al*., Thermal Infrared Imaging Experiments of C-Type Asteroid 162173 Ryugu on Hayabusa2. *Space Sci. Rev.* **208**, 255–286 (2017). doi: 10.1007/s11214-016-0286-8
8. Materials and methods are available as supplementary materials.
9. S. Tardivel, P. Sánchez, D. J. Scheeres, Equatorial cavities on asteroids, an evidence of fission events. *Icarus* **304**, 192–208 (2018). doi: 10.1016/j.icarus.2017.06.037
10. P. Michel, M. Delbo, Orbital and thermal evolutions of four potential targets for a sample return space mission to a primitive near-Earth asteroid. *Icarus* **209**, 520–534 (2010). doi: 10.1016/j.icarus.2010.05.013
11. N. Hirata *et al*., A survey of possible impact structures on 25143 Itokawa. *Icarus* **200**, 486–502 (2009). doi: 10.1016/j.icarus.2008.10.027
12. V. R. Oberbeck, W. L. Quaide, Genetic Implications of Lunar Regolith Thickness Variations. *Icarus* **9**, 446–465 (1968). doi: 10.1016/0019-1035(68)90039-0
13. C. Güttler, N. Hirata, A. M. Nakamura, Cratering experiments on the self armoring of coarse-grained granular targets. *Icarus* **220**, 1040–1049 (2012). doi: 10.1016/j.icarus.2012.06.041
14. E. Tatsumi, S. Sugita, Cratering efficiency on coarse-grain targets: Implications for the dynamical evolution of asteroid 25143 Itokawa. *Icarus* **300**, 227–248 (2018). doi: 10.1016/j.icarus.2017.09.004
15. W. F. Bottke *et al*., In search of the source of asteroid (101955) Bennu: Applications of the stochastic YORP model. *Icarus* **247**, 191–217 (2015). doi: 10.1016/j.icarus.2014.09.046
16. P. Michel, D. P. O'Brien, S. Abe, N. Hirata, Itokawa's cratering record as observed by Hayabusa: Implications for its age and collisional history. *Icarus* **200**, 503–513 (2009). doi: 10.1016/j.icarus.2008.04.002
17. S. Watanabe *et al*., Hayabusa2 arrives at the carbonaceous asteroid 162173 Ryugu—A spinning top–shaped rubble pile. *Science* **364**, 268–272 (2019). doi: 10.1126/science.aav8032
18. M. Ishiguro *et al*., Optical properties of (162173) 1999 JU3: In preparation for the JAXA Hayabusa2 sample return mission. *Astrophys. J.* **792**, 74 (2014). doi: 10.1088/0004-637X/792/1/74
19. S. J. Bus, R. P. Binzel, Phase II of the small main-belt asteroid spectroscopic survey: A feature-based taxonomy. *Icarus* **158**, 146–177 (2002). doi: 10.1006/icar.2002.6856
20. R. P. Binzel *et al*., Spectral Properties of Near-Earth Objects: Palomar and IRTF Results for 48 Objects Including Spacecraft Targets (9969) Braille and (10302) 1989 ML. *Icarus* **151**, 139–149 (2001). doi: 10.1006/icar.2001.6613
21. F. Vilas, Spectral characteristics of Hayabusa 2 Near-Earth asteroid targets 162173 1999 JU3 and 2001 QC34. *Astron. J.* **135**, 1101–1105 (2008). doi: 10.1088/0004-6256/135/4/1101
22. D. Lazzaro *et al*., Rotational spectra of (162173) 1999 JU3, the target of the Hayabusa2 mission. *Astron. Astrophys.* **549**, L2 (2013). doi: 10.1051/0004-6361/201220629
23. D. Morate *et al*., Compositional study of asteroids in the Erigone collisional family using visible spectroscopy at the 10.4 m GTC. *Astron. Astrophys.* **586**, A129 (2016). doi: 10.1051/0004-6361/201527453
24. K. Kitazato *et al*., The surface composition of asteroid 162173 Ryugu from Hayabusa2 near-infrared spectroscopy. *Science* **364**, 272–275 (2019). doi: 10.1126/science.aav7432
25. J. de León *et al*., Expected spectral characteristics of (101955) Bennu and (162173) Ryugu, targets of the OSIRIS-REx and Hayabusa2 missions. *Icarus* **313**, 25–37 (2018). doi: 10.1016/j.icarus.2018.05.009
26. T. Hiroi, M. E. Zolensky, C. M. Pieters, M. E. Lipschutz, Thermal metamorphism of the C, G, B, and F asteroids seen from the 0.7 μm, 3 μm, and UV absorption strengths in comparison with carbonaceous chondrites. *Meteorit. Planet. Sci.* **31**, 321–327 (1996). doi: 10.1111/j.1945-5100.1996.tb02068.x

ILLUSTRATION: YOSHIKO BABA

27. E. Tonui *et al*., Petrographic, chemical and spectroscopic evidence for thermal metamorphism in carbonaceous chondrites I: CI and CM chondrites. *Geochim. Cosmochim. Acta* **126**, 284–306 (2014). doi: 10.1016/j.gca.2013.10.053
28. P. Vernazza *et al*., Interplanetary dust particles as samples of icy asteroids. *Astrophys. J.* **806**, 204 (2015). doi: 10.1088/0004-637X/806/2/204
29. S. Fornasier, C. Lantz, M. A. Barucci, M. Lazzarin, Aqueous alteration on main belt primitive asteroids: Results from visible spectroscopy. *Icarus* **233**, 163–178 (2014). doi: 10.1016/j.icarus.2014.01.040
30. J. M. Bauer *et al*., The NEOWISE-Discovered Comet Population and the CO + CO_2, Production Rates. *Astrophys. J.* **814**, 85 (2015). doi: 10.1088/0004-637X/814/2/85
31. B. E. Clark *et al*., NEAR Photometry of asteroid 253 Mathilde. *Icarus* **140**, 53–65 (1999). doi: 10.1006/icar.1999.6124
32. E. A. Cloutis, P. Hudon, T. Hiroi, M. J. Gaffey, Spectral reflectance properties of carbonaceous chondrites 4: Aqueously altered and thermally metamorphosed meteorites. *Icarus* **220**, 586–617 (2012). doi: 10.1016/j.icarus.2012.05.018
33. T. Nakamura, Post-hydration thermal metamorphism of carbonaceous chondrites. *J. Mineral. Petrol. Sci.* **100**, 260–272 (2005). doi: 10.2465/jmps.100.260
34. E. A. Cloutis, T. Hiroi, M. J. Gaffey, C. M. O. D. Alexander, P. Mann, Spectral reflectance properties of carbonaceous chondrites: 1. CI chondrites. *Icarus* **212**, 180–209 (2011). doi: 10.1016/j.icarus.2010.12.009
35. E. A. Cloutis, P. Hudon, T. Hiroi, M. J. Gaffey, P. Mann, Spectral reflectance properties of carbonaceous chondrites: 2. CM chondrites. *Icarus* **216**, 309–346 (2011). doi: 10.1016/j.icarus.2011.09.009
36. M. Delbo *et al*., Thermal fatigue as the origin of regolith on small asteroids. *Nature* **508**, 233–236 (2014). doi: 10.1038/nature13153; pmid: 24695219
37. S. Marchi, M. Delbo', A. Morbidelli, P. Paolicchi, M. Lazzarin, Heating of near-Earth objects and meteoroids due to close approaches to the Sun. *Mon. Not. R. Astron. Soc.* **400**, 147–153 (2009). doi: 10.1111/j.1365-2966.2009.15459.x
38. S. C. Koga *et al*., Spectral decomposition of asteroid Itokawa based on principal component analysis. *Icarus* **299**, 386–395 (2018). doi: 10.1016/j.icarus.2017.08.016
39. T. G. Müller *et al*., Hayabusa-2 mission target asteroid 162173 Ryugu (1999 JU3): Searching for the object's spin-axis orientation. *Astron. Astrophys.* **599**, A103 (2017). doi: 10.1051/0004-6361/201629134
40. N. Sakatani *et al*., Thermal conductivity model for powdered materials under vacuum based on experimental studies. *AIP Adv.* **7**, 015310 (2017). doi: 10.1063/1.4975153
41. E. Cloutis *et al*., Spectral reflectance "deconstruction" of the Murchison CM2 carbonaceous chondrite and implications for spectroscopic investigations of dark asteroids. *Icarus* **305**, 203–224 (2018). doi: 10.1016/j.icarus.2018.01.015
42. T. Michikami *et al*., Size-frequency statistics of boulders on global surface of asteroid 25143 Itokawa. *Earth Planets Space* **60**, 13–20 (2008). doi: 10.1186/BF03352757
43. P. C. Thomas, J. Veverka, M. S. Robinson, S. Murchie, Shoemaker crater as the source of most ejecta blocks on the asteroid 433 Eros. *Nature* **413**, 394–396 (2001). doi: 10.1038/35096513; pmid: 11574880
44. S. Mazrouei, M. G. Daly, O. S. Barnouin, C. M. Ernst, I. DeSouza, Block distribution on Itokawa. *Icarus* **229**, 181–189 (2014). doi: 10.1016/j.icarus.2013.11.010
45. Y. Jiang *et al*., Boulders on asteroid Toutatis as observed by Chang'e-2. *Sci. Rep.* **5**, 16029 (2015). doi: 10.1038/srep16029; pmid: 26522880
46. H. Demura *et al*., Pole and global shape of 25143 Itokawa. *Science* **312**, 1347–1349 (2006). doi: 10.1126/science.1126574; pmid: 16741112
47. H. Miyamoto *et al*., Regolith migration and sorting on asteroid Itokawa. *Science* **316**, 1011–1014 (2007). doi: 10.1126/science.1134390; pmid: 17446355
48. J. Veverka *et al*., Imaging of small-scale features on 433 Eros from NEAR: Evidence for a complex regolith. *Science* **292**, 484–488 (2001). doi: 10.1126/science.1058651; pmid: 11313490
49. A. Bischoff *et al*., "Nature and origins of meteoritic breccias" in *Meteorites and the Early Solar System II*, D. S. Lauretta, H. Y. McSween Jr., Eds. (Univ. of Arizona Press, 2006), pp. 679–712.
50. P. Michel *et al*., Selective sampling during catastrophic disruption: Mapping the location of reaccumulated fragments in the original parent body. *Planet. Space Sci.* **107**, 24–28 (2015). doi: 10.1016/j.pss.2014.08.005
51. S. Wakita, M. Sekiya, Thermal Evolution of Icy Planetesimals in the Solar Nebula. *Earth Planets Space* **63**, 1193–1206 (2011). doi: 10.5047/eps.2011.08.012
52. G. D. Cody *et al*., Organic thermometry for chondritic parent bodies. *Earth Planet. Sci. Lett.* **272**, 446–455 (2008). doi: 10.1016/j.epsl.2008.05.008
53. F. Herbert, C. P. Sonett, M. J. Gaffey, "Protoplanetary thermal metamorphism: The hypothesis of electromagnetic induction in the protosolar wind" in *The Sun in Time* (Univ. of Arizona Press, 1991), pp. 710–739.
54. W. F. Bottke Jr., M. C. Nolan, R. Greenberg, R. A. Kolvoord, Velocity distributions among colliding asteroids. *Icarus* **107**, 255–268 (1994). doi: 10.1006/icar.1994.1021
55. N. A. Moskovitz *et al*., Rotational characterization of Hayabusa II target Asteroid (162173) 1999 JU3. *Icarus* **224**, 24–31 (2013). doi: 10.1016/j.icarus.2013.02.009
56. S. J. Bus, R. P. Binzel, Phase II of the small main-belt asteroid spectroscopic survey: The observations. *Icarus* **158**, 106–145 (2002). doi: 10.1006/icar.2002.6857
57. M. Matsuoka *et al*., An evaluation method of reflectance spectra to be obtained by Hayabusa2 Near-Infrared Spectrometer (NIRS3) based on laboratory measurements of carbonaceous chondrites. *Earth Planets Space* **69**, 120 (2017). doi: 10.1186/s40623-017-0705-4
58. C. M. Pieters, Strength of mineral absorption features in the transmitted component of near-infrared reflected light: First results from RELAB. *J. Geophys. Res.* **88**, 9534–9544 (1983). doi: 10.1029/JB088iB11p09534
59. M. Matsuoka *et al*., Pulse-laser irradiation experiments of Murchison CM2 chondrite for reproducing space weathering on C-type asteroids. *Icarus* **254**, 135–143 (2015). doi: 10.1016/j.icarus.2015.02.029

ACKNOWLEDGMENTS

We thank the anonymous reviewers for their helpful comments. The Hayabusa2 spacecraft was developed and built under the leadership of Japan Aerospace Exploration Agency (JAXA), with contributions from the German Aerospace Center (DLR) and the Centre National d'Études Spatiales (CNES), and in collaboration with NASA, Nagoya University, University of Tokyo, National Astronomical Observatory of Japan (NAOJ), University of Aizu, Kobe University, and other universities, institutes, and companies in Japan. We also thank many engineers, including N. Inaba at JAXA and T. Masuda, S. Yasuda, K. Matsushima, and T. Ohshima at NEC Corp. for their dedicated work on the Hayabusa2 mission; K. Sato at NEC Corp. for ONC development; S. Kashima at NAOJ for optical calculations; and Y. Baba at UTOPS for illustrating Fig. 8. **Funding:** This study was supported by KAKENHI from the Japanese Society for Promotion of Science (JSPS) (grants JP25120006, 17H01175, JP17H06459, JP17K05639, JP16H04059, JP17KK0097, JP26287108, and JP16H04044) and the JSPS Core-to-Core program "International Network of Planetary Sciences." P.M. and M.A.B. acknowledge funding support from the French space agency CNES. P.S. acknowledges funding from the Complex Systems Academy of Excellence and the Space, Environment, Risk, and Resilience Academy of Excellence, part of the IDEX JEDI of the Université Côte d'Azur in connection with its Center for Planetary Origin. T.M. has received funding from the European Union's Horizon 2020 Research and Innovation Programme (Grant 687378). D.D.L., C.M.E., L.L.C., and M.K. acknowledge funding through the NASA Hayabusa2 Participating Scientist Program. **Author contributions:** S.Su. coordinated coauthor contributions; led the ONC data acquisition, analyses, and interpretations; and wrote the paper, with contributions from D.D., T.Ok., N.Na., T.Mo., and R.-L.B. ONC data acquisitions and reductions: R.Ho., T.Mo., Y.Ii., S.Ka. H.Sa., E.T., C.Ho., Y.Yo., M.Ya., T.K., N.Sa., K.Og., H.Su., K.Yoshio., M.Ha., Y.C., M.M., D.D., and H.K. Geomorphology analyses: H.M., T.Mo., E.T., C.Ho., T.Mi., Y.C., M.Hi., P.M., O.S.B., C.M.E., L.L.C., S.E.S., R.J., K.Ot., N.Sc., H.K., R.He., G.K., T.Mic., S.Sa., and P.A.A. Spectral analysis: E.T., D.D., R.Ho., Y.Yo., T.Mo., C.S., N.T., Y.Su., S.Ha., M.I., S.Tac., M.O., K.Na., M.E.Z., F.V., and M.A.B. TIR data acquisitions and analyses: T.Ok., T.F., S.Tan., M.T., T.A., H.Se., H.D., Y.Og., T.K., N.Sa., Y.Sh., T.Se., T.G.M., and A.Ha. LIDAR data acquisitions and analyses: N.Na, T.Miz., H.Se., H.N., K.M., N.H. (Kobe), R.Y., Y.Is., H.I., H.A., K.Ya., S.A., F.Y., A.Hi., S.Sa, S.O., S.Ts., K.A., S.Ta., M.S., H.M., H.D., J.K., T.Ot.; Shape modeling: N.H. (Kobe), N.H. (Aizu), R.N., E.P., R.G., O.S.B., C.M.E., and S.W. 3D numerical calculations: R.-L.B. Interpretation and writing contribution: T.Mo., E.T., D.D., R.Ho, T.Ok., N.Na., T.N., T.H., P.M., O.S.B., C.M.E., S.E.S., H.Yab., M.E.Z., S.W., and M.F. Science operations of spacecraft: S.Tan., M.Yo., T.I., M.A., M.Ha., T.Ok., R.N., Y.Sh., N.Sa., M.M., H.Yan., R.T., M.O., F.T., N.O., H.Sa., T.Y., S.Ki., Y.Ok., Y.Taka., H.T., G.O., Y.Mi., K.Yoshik., T.T., Y.Take., A.F., C.Hi., S.N., S.Ho., O.M., T.Sh., S.So., K.Ni., T.S., and Y.Ts. **Competing interests:** Y.Ya. is also affiliated with Tokyo Metropolitan University. **Data and materials availability:** All images, new software, and input data used in this study are available at the JAXA Data Archives and Transmission System (DARTS) at www.darts.isas.jaxa.jp/pub/hayabusa2/paper/Sugita_2019/. Additional data from the mission will be delivered to the DARTS archive at www.darts.isas.jaxa.jp/planet/project/hayabusa2/, and higher-level data products will be available in the Small Bodies Node of the NASA Planetary Data System (https://pds-smallbodies.astro.umd.edu/) 1 year after mission departure from the asteroid.

SUPPLEMENTARY MATERIALS

13 November 2018; accepted 12 March 2019
Published online 19 March 2019
10.1126/science.aaw0422

Science

The geomorphology, color, and thermal properties of Ryugu: Implications for parent-body processes

S. Sugita, R. Honda, T. Morota, S. Kameda, H. Sawada, E. Tatsumi, M. Yamada, C. Honda, Y. Yokota, T. Kouyama, N. Sakatani, K. Ogawa, H. Suzuki, T. Okada, N. Namiki, S. Tanaka, Y. Iijima, K. Yoshioka, M. Hayakawa, Y. Cho, M. Matsuoka, N. Hirata, N. Hirata, H. Miyamoto, D. Domingue, M. Hirabayashi, T. Nakamura, T. Hiroi, T. Michikami, P. Michel, R.-L. Ballouz, O. S. Barnouin, C. M. Ernst, S. E. Schröder, H. Kikuchi, R. Hemmi, G. Komatsu, T. Fukuhara, M. Taguchi, T. Arai, H. Senshu, H. Demura, Y. Ogawa, Y. Shimaki, T. Sekiguchi, T. G. Müller, A. Hagermann, T. Mizuno, H. Noda, K. Matsumoto, R. Yamada, Y. Ishihara, H. Ikeda, H. Araki, K. Yamamoto, S. Abe, F. Yoshida, A. Higuchi, S. Sasaki, S. Oshigami, S. Tsuruta, K. Asari, S. Tazawa, M. Shizugami, J. Kimura, T. Otsubo, H. Yabuta, S. Hasegawa, M. Ishiguro, S. Tachibana, E. Palmer, R. Gaskell, L. Le Corre, R. Jaumann, K. Otto, N. Schmitz, P. A. Abell, M. A. Barucci, M. E. Zolensky, F. Vilas, F. Thuillet, C. Sugimoto, N. Takaki, Y. Suzuki, H. Kamiyoshihara, M. Okada, K. Nagata, M. Fujimoto, M. Yoshikawa, Y. Yamamoto, K. Shirai, R. Noguchi, N. Ogawa, F. Terui, S. Kikuchi, T. Yamaguchi, Y. Oki, Y. Takao, H. Takeuchi, G. Ono, Y. Mimasu, K. Yoshikawa, T. Takahashi, Y. Takei, A. Fujii, C. Hirose, S. Nakazawa, S. Hosoda, O. Mori, T. Shimada, S. Soldini, T. Iwata, M. Abe, H. Yano, R. Tsukizaki, M. Ozaki, K. Nishiyama, T. Saiki, S. Watanabe and Y. Tsuda

Science **364** (6437), eaaw0422.
DOI: 10.1126/science.aaw0422originally published online March 19, 2019

Hayabusa2 at the asteroid Ryugu

Asteroids fall to Earth in the form of meteorites, but these provide little information about their origins. The Japanese mission Hayabusa2 is designed to collect samples directly from the surface of an asteroid and return them to Earth for laboratory analysis. Three papers in this issue describe the Hayabusa2 team's study of the near-Earth carbonaceous asteroid 162173 Ryugu, at which the spacecraft arrived in June 2018 (see the Perspective by Wurm). Watanabe *et al.* measured the asteroid's mass, shape, and density, showing that it is a "rubble pile" of loose rocks, formed into a spinning-top shape during a prior period of rapid spin. They also identified suitable landing sites for sample collection. Kitazato *et al.* used near-infrared spectroscopy to find ubiquitous hydrated minerals on the surface and compared Ryugu with known types of carbonaceous meteorite. Sugita *et al.* describe Ryugu's geological features and surface colors and combined results from all three papers to constrain the asteroid's formation process. Ryugu probably formed by reaccumulation of rubble ejected by impact from a larger asteroid. These results provide necessary context to understand the samples collected by Hayabusa2, which are expected to arrive on Earth in December 2020.

Science, this issue p. 268, p. 272, p. eaaw0422; see also p. 230

Science (print ISSN 0036-8075; online ISSN 1095-9203) is published by the American Association for the Advancement of Science, 1200 New York Avenue NW, Washington, DC 20005.